Finite Element Flow Simulations for Three-Dimensional Incompressible Viscous Fluid

Kazuhiko Kakuda and Naoki Hara
Department of Mathematical Information Engineering,
College of Industrial Technology,
Nihon University, Chiba 275-8575, Japan
E-mail:k7kakuda@cit.nihon-u.ac.jp

Summary

The applications of a finite element scheme to three-dimensional incompressible viscous fluid flows are presented. The scheme is based on the Petrov-Galerkin weak formulation with exponential weighting functions. The incompressible Navier-Stokes equations are numerically integrated in time by using a fractional step strategy with second-order accurate Adams-Bashforth scheme for both advection and diffusion terms. Numerical solutions for flow around a circular cylinder and flow around an insulator of a pantograph are presented.

Introduction

From a practical point of view, the numerical simulations of three-dimensional viscous fluid flows up to high Reynolds number are indispensable in science and engineering fields. Numerical instabilities have been experienced in the solution of incompressible Navier-Stokes equations at a high Reynolds number [1]. To stabilize such calculations, various upwind schemes have been successfully presented in finite difference and finite element frameworks [2,3].

We have developed a finite element scheme based on the Petrov-Galerkin weak formulation using exponential weighting functions for solving accurately and in a stable manner the flow field of an incompressible viscous fluid up to high Reynolds number regimes [4,5]. The Navier-Stokes equations are semi-explicitly integrated in time by using a fractional step strategy, and hence split into the advection-diffusion eqution and linear Euler-type equtions. As the time-marching scheme, we adopt effectively the second-order accurate Adams-Bashforth explicit differencing for both advection and diffusion terms.

The purpose of this paper is to present the application of the Petrov-Galerkin finite element scheme using exponential weighting functions to various flow problems in three-dimensional incompressible viscous fluid. The workability and validity of the present approach are demonstrated through flow around a circular cylinder [6-12] and flow around an insulator of a pantograph [13,14] up to high Reynolds number.

Statement of the Problem

The motion of an incompressible viscous fluid flow is governed by the Navier-Stokes equations in dimensionless form. By applying the time splitting technique to the set of equations, we can split formally the problem into the following two parts :

$$\dot{u}_i(\tilde{u}_i, u_i^n) + u_j u_{i,j} = \frac{1}{Re} u_{i,jj} \qquad in\ \Im \times \Omega \tag{1}$$

$$\dot{u}_i(u_i^{n+1}, \tilde{u}_i) = -p_{,i}\ ,\ u_{i,i} = 0 \qquad in\ \Im \times \Omega \tag{2}$$

In these expressions, u_i is the velocity vector component, p is the pressure, Re is the Reynolds number, $\tilde{u}_i$ is the auxiliary velocity vector, and u_i^n denotes the value of u_i at time level $n\Delta t$, where Δt is a time increment.

Finite Element Formulation

Proceedings of the 2004 International Conference on Computational & Experimental Engineering & Science 26-29 July, 2004, Madeira, Portugal

Let us now consider the Petrov-Galerkin finite element formulation using exponential weighting functions [4] to equation (1). By applying the divergence theorem to the weighted residual form of equation (1), and after some manipulations, we have the following weak form :

$$\int_{\Omega_e} \{\dot{u}_i(\tilde{u}_i, u_i^n) + u_j u_{i,j}\} M_\alpha d\Omega + \int_{\Omega_e} \frac{1}{Re} u_{i,j} N_{\alpha,j} d\Omega = \int_{\Gamma_e} \tau_i N_\alpha d\Gamma \tag{3}$$

where $\tau_i \equiv u_{i,j} n_j / Re$, Ω_e is a subdomain of the whole domain Ω, Γ_e is the boundary on the subdomain, and M_α denotes the weighting function given by

$$\left.\begin{aligned} M_\alpha(\boldsymbol{x}) &= \sum_{\gamma,i} N_\alpha(\boldsymbol{x}) e^{-a_i(N_\gamma x_i^\gamma - x_i^\alpha)} \\ a_i &= \frac{\alpha_i}{\mid L_i \mid} sgn(v_i) \end{aligned}\right\} \tag{4}$$

where N_α is the shape function in three dimensions, v_i is the velocity vector averaged in Ω_e, L_i is the reference length for x_i-directions, α_i is the scaling parameters which control an effect of the upwinding, and $sgn(v_i)$ denotes the signum function.

At this stage, by using the second-order accurate Adams-Bashforth strategy as a time integration scheme, we have the following finite element system of equations :

$$\mathrm{M}_{\alpha\beta} \frac{\{\tilde{u}_i\}_\beta - \{u_i^n\}_\beta}{\Delta t} = \frac{1}{2}(3\mathrm{F}_{i\alpha}^n - \mathrm{F}_{i\alpha}^{n-1}) \tag{5}$$

in which $\mathrm{M}_{\alpha\beta}$ is the so-called mass matrix, and $\mathrm{F}_{i\alpha}^n$ is given by

$$\mathrm{F}_{i\alpha}^n = -\mathrm{K}_{\alpha\beta}(u_j^n)\{u_i^n\}_\beta - \mathrm{D}_{\alpha\beta}\{u_i^n\}_\beta + \mathrm{f}_{i\alpha}^n \tag{6}$$

where each matrix is defined in reference [5].

On the other hand, the conventional Galerkin finite element formulation can be applied to solve numerically the set of equation (2).

Numerical Examples

In this section we present numerical results obtained from applications of the above-mentioned numerical method to incompressible viscous flow problems. In our numerical performances, we adopt the lowest interpolation functions in which the velocity and the scalar potential are piecewise trilinear, and the pressure is constant over each element. The initial velocities are assumed to be zero everywhere in the interior domain.

Flow around a circular cylinder

We shall consider the flow around a circular cylinder. Fig.1 shows the geometry, the boundary conditions, and the finite element mesh of the flow around a circular cylinder. The Reynolds number, Re, based on the uniform velocity, U_0, at the inflow and the cube height, D, is 10^3. The parameters that characterize the finite element approximation are summarized in Table 1.

Fig.2(a) shows the instantaneous streamlines around the cylinder in horizontal x_1x_2-section at $x_3 = 2.0$ and vertical x_1x_3-section at $x_2 = 10.0$ for $Re = 10^3$. The corresponding pressure fields are shown in Fig.2(b). It is clear from the streamlines that the periodic flow pattern appears in the direction of the vertical axis of the cylinder. From the pressure fields, there appear to have the longitudinal vortices in the downstream region of the cylinder. Fig.3 shows the time histories of the drag and lift coefficients, and the power spectrum for the lift coefficient. In Table 2 and Fig.4 we give the time-averaged drag coefficient, $\overline{C}_d$, and the Strouhal number, S_t, through comparison with experimental data and other numerical solutions. Our numerical results for $Re = 10^3$ are in good agreement with the experimental data.

Table 1 A summary of the parameters

Re	Nodes	Elements	l_{min}	$\triangle t$	α_i
10^3	179,970	168,000	0.00341	0.002	0.4

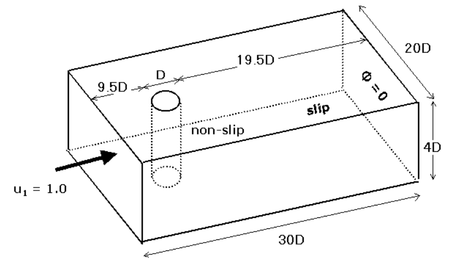

(a) Geometry and boundary conditions

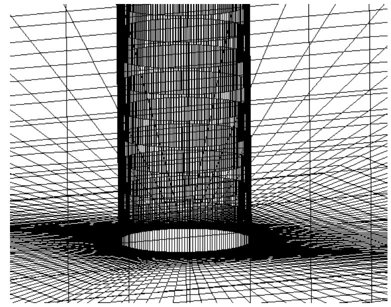

(b) Finite element mesh

Figure 1: Flow around a circular cylinder

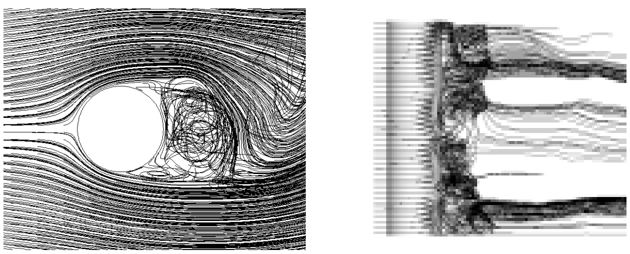

(a) Streamlines

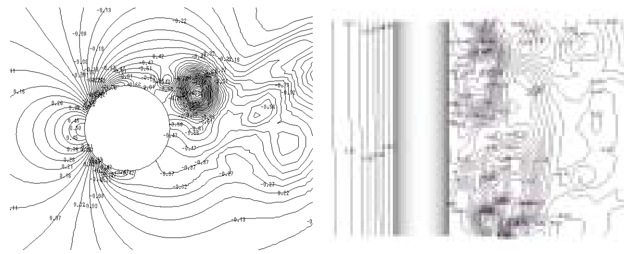

(b) Pressure fields

Figure 2: Instantaneous streamlines and pressure fields for $Re = 10^3$

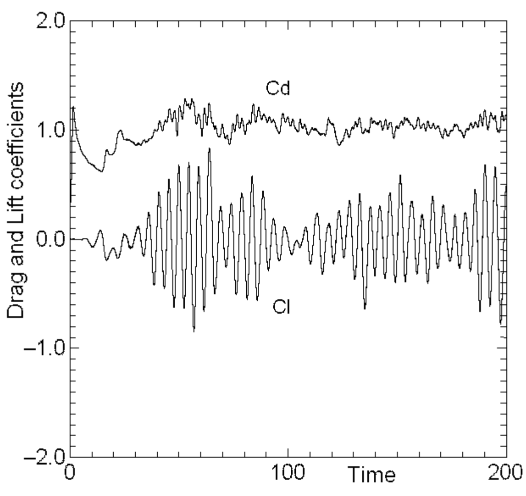

(a) Time histories of C_d and C_l

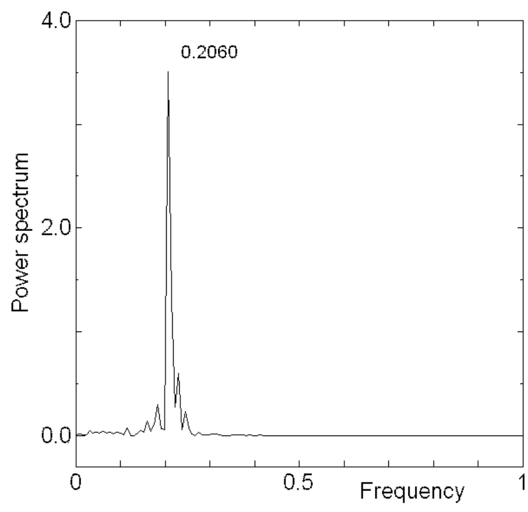

(b) Power spectrum for C_l

Figure 3: Time histories of drag and lift coefficients, and the power spectrum

Table 2 Comparisons of $\overline{C}_d$ and S_t

	$\overline{C}_d$	S_t
present	1.028	0.2060
Kieda et al.: FDM [9]	1.18	0.191
Harada & Kashiyama: FEM [10]	1.05	0.229
Ueki & Ogura: CIP-FEM [11]	1.10	0.214
Braza, Chassaing & Minh (2D) [12]	1.198	0.21
Experimental data [6, 7]	1.0	0.19∼0.22

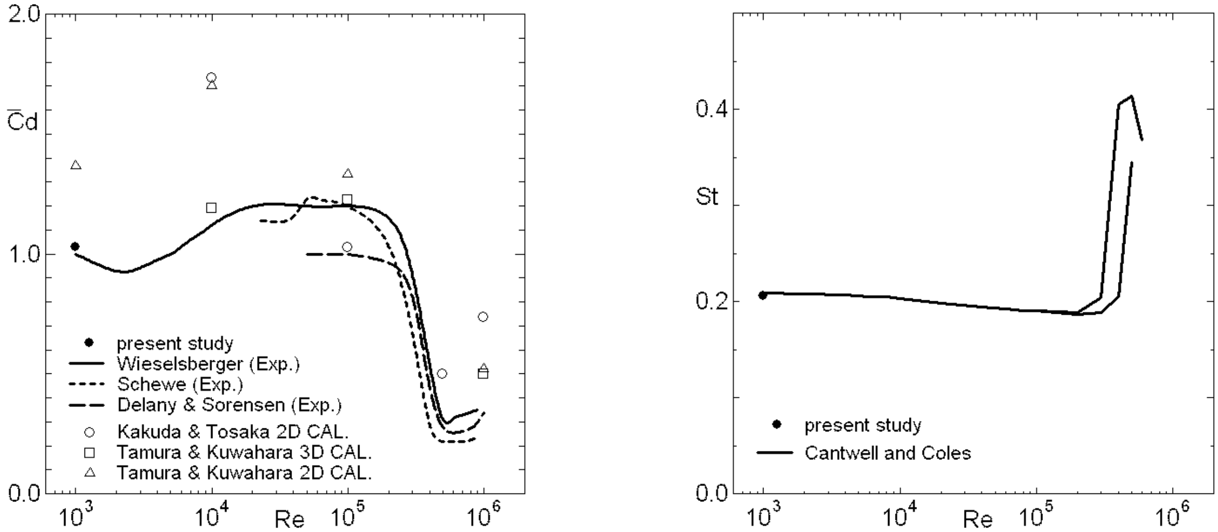

(a) Time-averaged drag coefficient

(b) Strouhal number

Figure 4: Time-averaged drag coefficient and Strouhal number

Flow around an insulator of a pantograph

As the second example, we shall consider the flow around an insulator of a pantograph. Fig.5 shows the geometry, the boundary conditions, and the finite element mesh of the flow around an insulator of a pantograph. The Reynolds numbers, Re, based on the uniform velocity, U_0, at the inflow and the diameter of the insulator, D, are 10^3 and 10^6, respectively. The parameters that characterize the finite element approximation are summarized in Table 3.

Fig.6 shows the instantaneous streamlines around rear and side surfaces of the insulator for $Re = 10^3$ and 10^6. The corresponding pressure fields are shown in Fig.7. From the streamlines at $Re = 10^6$(see Fig.6(b)), there appears to have the flow behavior in x_3-direction behind the insulater. It is also clear from the pressure field(see Fig.7(b)) that the longitudinal vortices are appeared in the downstream region of the insulator. In Fig.8 we give the comparisons of the distribution of Powell's sound source term, $\nabla \cdot (\boldsymbol{\omega} \times \boldsymbol{u})$, with other finite element results [13]. The Powell's sound source term is a value acquired from the right-hand side of Powell equation, $\partial^2\rho/\partial t^2 - a_0^2\nabla^2\rho = \rho_0\nabla \cdot (\boldsymbol{\omega} \times \boldsymbol{u})$. Our numerical results are similar to the finite element data. It turns out that the noises occur mainly near the rear and side regions of the insulator.

Table 3 A summary of the parameters

Case	Re	Nodes	Elements	l_{min}	Δt	α_i
1	10^3	154,741	144,800	0.051	0.01	0.6
2	10^6	372,526	358,400	0.01	0.005	0.6

Conclusions

We have presented a finite element scheme for solving numerically three-dimensional incompressible Navier-Stokes equations. The scheme is based on the Petrov-Galerkin finite element formulation using exponential weighting functions. The set of equations is numerically integrated in time by using the second-order accurate Adams-Bashforth strategy for both advection and diffusion terms.

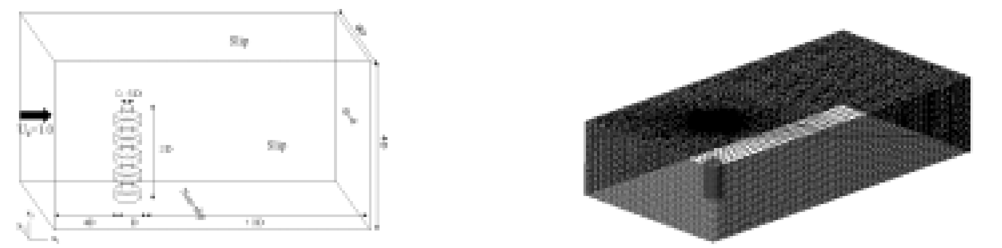

(a) Geometry and boundary conditions (b) Finite element mesh (case 2)

Figure 5: Flow around an insulator of a pantograph

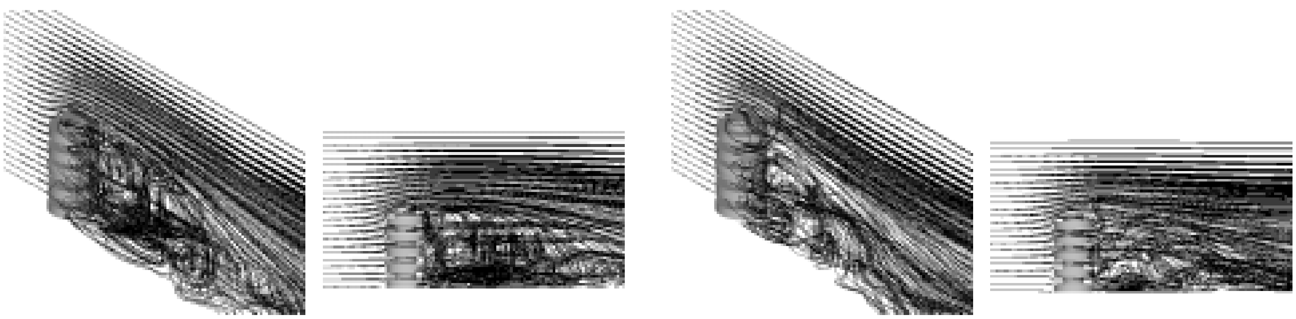

(a) $Re = 10^3$ (b) $Re = 10^6$

Figure 6: Instantaneous streamlines

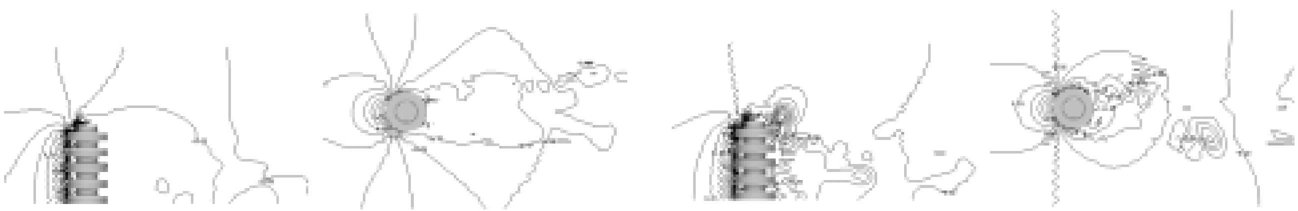

(a) $Re = 10^3$ (b) $Re = 10^6$

Figure 7: Instantaneous pressure fields

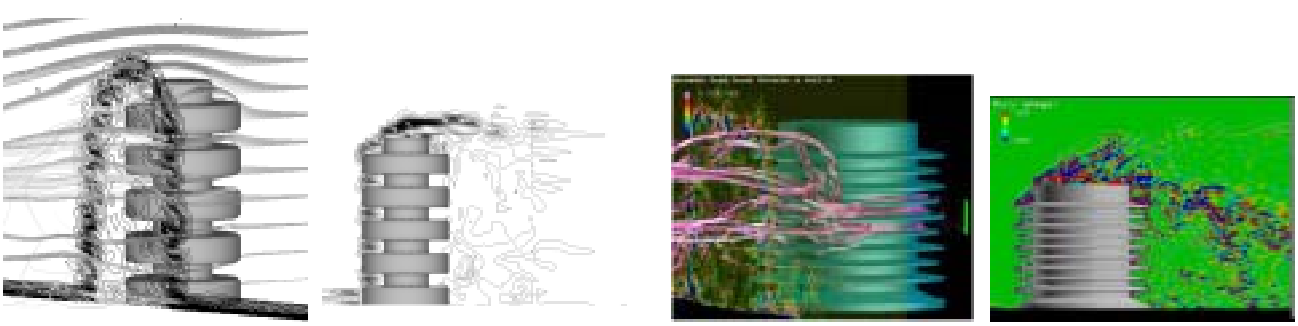

(a) Present results for $Re = 10^6$ (b) Kato,et al.:FEM[14]

Figure 8: Distribution of the sound source

As the numerical examples, flow around a circular cylinder and flow around an insulator of a pantograph were simulated up to high Reynolds number regimes. The numerical results for flow around a circular cylinder are quantitatively in good agreement with experimental data. The numerical results also demonstrate that the present approach is capable of solving three-dimensional incompressible Navier-Stokes equations in a stable manner up to high Reynolds numbers.

Acknowledgments

This research was supported by a Grant from the Ministry of Education, Culture, Sports, Science, and Technology to promote advanced scientific research.

References

1. Peyret, R. and Taylor, T.D. (1983): *Computational Methods for Fluid Flow*, Springer-Verlag, New York.

2. Fletcher, C.A.J. (1991): *Computational Techniques for Fluid Dynamics*, Vols.I, , Springer-Verlag, Tokyo.

3. Pironneau, O. (1989): *Finite Element Methods for Fluids*, John Wiley & Sons, New York.

4. Kakuda, K. and Tosaka, N. (1992): "Finite Element Approach for High Reynolds Number Flows", *Theoretical and Applied Mechanics*, **41**, pp.223-232.

5. Kakuda, K., Tosaka, N. and Nakamura, T. (1996): "Finite Element Analysis for 3-D High Reynolds Number Flows", *Int. J. Comp. Fluid Dyn.*, **7**, pp.163-178.

6. Wieselsberger, C. (1921): "Neuere Feststellungen über die Gesetze des Flüssigkeits- und Luftwiderstandes", *Physik. Zeitschr.*, **XXII**, pp.321-328.

7. Cantwell, B. and Coles, D. (1983): "A Experimental Study of Entrainment and Transport in the Turbulent near Wake of a Circular Cylinder", *J. Fluid Mech.* **136**, pp.321-374.

8. Tamura, T. and Kuwahara, K. (1989): "Direct Finite Difference Computation of Turbulent Flow around a Circular Cylinder", *Num. Meths. Fluid Dyns.* , (Eds., M. Yasuhara *et al.*), pp.645-650.

9. Kieda, K., Taniguchi, N., Matsumiya, H. and Kobayashi, T. (1997): "Numerical Simulation of 3D Flow around a Circular Cylinder (1st Report, Analysis of Time and Space Correlation)", (in Japanease), *Tran. JSME*, B, $\mathbf{63-614}$, pp.3231-3238.

10. Harada, T. and Kashiyama, K. (1998): "Stabilized Finite Element Analysis of Three-Dimensional Flow around a Circular Cylinder", (in Japanese), *Proc. Twelfth Symp. CFD*, pp.481-482.

11. Ueki, H. and Ogura, K. (1998): "Application of CIP-FEM to Three-Dimensional Unsteady Incompressible Flow", (in Japanese), *Proc. Twelfth Symp. CFD*, pp.337-338.

12. Braza, M., Chassaing, P. and Minh, H.H. (1986): "Numerical Study and Physical Analysis of the Pressure and Velocity Fields in the near Wake of a Circular Cylinder", *J. Fluid Mech.*, **165**, pp.79-130.

13. Powell, A. (1964): "Theory of vortex sound", *J. Acoust. Soc. Am*, **36**, pp.177-195.

14. Kato, C., Shimizu, H., Mukai, H. and Okamura, T. (1999): "Large Eddy Simulation of Aeroacoustic Source Distribution in a Wake of Three-dimensional Body", (in Japanese), *Proc. Thirteenth Symp. CFD*, CD-ROM.